NUMERICAL CALCULATION OF BEAM COUPLING IMPEDANCES IN THE FREQUENCY DOMAIN USING FIT*

U. Niedermayer# and O. Boine-Frankenheim
Technische Universität Darmstadt, Institut für Theorie Elektromagnetischer Felder (TEMF),
Schlossgartenstraße 8, 64289 Darmstadt, Germany

Abstract

The transverse impedance of kicker magnets is considered to be one of the main beam instability sources in the projected SIS-100 at FAIR and also in the SPS at CERN. The longitudinal impedance can contribute to the heat load, which is especially a concern in the cold sections of SIS-100 and LHC. In the high frequency range, commercially available time domain codes like CST Particle Studio serve to calculate the impedance but they are inapplicable at medium and low frequencies which become more important for larger size synchrotrons. We present the ongoing work of developing a Finite Integration Technique (FIT) solver in frequency domain which is based on the Parallel and Extensible Toolkit for Scientific computing (PETSc) framework in C++. Proper beam adapted boundary conditions are important to validate the concept. The code is applied to an inductive insert used to compensate the longitudinal space charge impedance in low energy machines. Another application focuses on the impedance contribution of a ferrite kicker with inductively coupled pulse forming network (PFN).

INTRODUCTION

For the SIS100 synchrotron which will be built in the framework of the FAIR project, especially the coasting beam and the high intensity proton bunch are susceptible to impedance driven coherent transverse instabilities. Since SIS100 is a cryogenic (< 20 K) machine, the beam induced heat load is an important issue. In the relevant frequency range of several kHz to 2 GHz impedance sources are mainly given by the thin stainless steel beam pipe [1] and ferrite components. Above the cut-off frequency of the beam pipe, wake fields are traveling off-phase with the beam such that no net interaction takes place in long bunches. Additionally to the necessary ferrite kickers and their supply networks, also an inductive ferrite insertion to compensate the negative inductive longitudinal space charge impedance has been proposed. The longitudinal and transverse impedances of these objects have to be quantified in order to ensure a stable high intensity beam by designing instability countermeasures.

Usually coupling impedances are defined as the Fourier transform of the wake function. The wake function can be calculated by commercial software such as CST Particle Studio [2]. At low frequencies, which become more important for large hadron synchrotrons, this technique is inapplicable. From Küpfmüller's uncertainty principle $\Delta t \Delta f \geq 1$ with some definition of the time-duration and bandwidth [3] one finds that 300 km of wake-length have to be integrated in order to obtain a frequency-resolution of 1 kHz. Therefore at low and medium frequencies a frequency domain (FD) approach is pursued. The problem of determining coupling impedances in the frequency domain has already been addressed by Doliwa et al. [4] using a Neumann series approach with a Python implementation. The new implementation described here is supposed to carry on this work on a more general C++ platform with properly defined interfaces to the PETSc [5] framework on modern 64-bit machines.

The following will give a definition of the coupling impedances directly in FD. By convention underlined symbols emphasize complex variables. This also serves to distinguish between time domain (TD) and frequency domain (FD) fields. The beam with total charge q in a synchrotron is modeled as a disc with radius a of uniform surface charge density σ traveling with velocity v. The transverse displacement d_x of the beam (i.e. a coherent dipole oscillation) is approximated to first order by

$$\sigma(\varrho,\varphi) \approx \frac{q}{\pi a^2}\left[\Theta(a-\varrho)+\delta(a-\varrho)d_x\cos\varphi\right] \quad (1)$$

$$=: \sigma_\parallel\Theta(a-\varrho)+\sigma_\perp\delta(a-\varrho) \quad (2)$$

where Θ is the unit step and δ is its generalized derivative. The beam's volume charge density is given by $\varrho(\vec{r},t) = \sigma(\varrho,\varphi)\delta(z-vt)$ and it reads in frequency domain

$$\underline{\varrho}(\vec{r},\omega) = \int_{-\infty}^{\infty}\varrho(\vec{r},t)e^{-i\omega t}\mathrm{d}t = \frac{1}{v}\sigma(\varrho,\varphi)e^{-i\omega z/v}. \quad (3)$$

The beam current density in frequency domain is

$$\underline{J}_{s,z}(\varrho,\varphi,z;\omega) = \sigma(\varrho,\varphi)e^{-i\omega z/v} =: \underline{J}_\parallel + \underline{J}_\perp \quad (4)$$

where $\underline{J}_\parallel$ and $\underline{J}_\perp$ are the monopole and dipole components, as in Eq. (2), respectively. The coherent force due to beam induced electromagnetic fields acting back on the beam is described by the coupling impedance [6]

$$\underline{Z}_\parallel(\omega) = -\frac{1}{q^2}\int_{\mathrm{beam}}\underline{\vec{E}}\cdot\underline{\vec{J}}_\parallel^*\,\mathrm{d}V \quad (5)$$

$$\underline{Z}_{\perp,x}(\omega) = -\frac{v}{(qd_x)^2\omega}\int_{\mathrm{beam}}\underline{\vec{E}}\cdot\underline{\vec{J}}_\perp^*\mathrm{d}V. \quad (6)$$

The electric field $\underline{\vec{E}}$ is to be calculated from Maxwell's equations. Instead of the cosine distribution for dipolar excitation in Eq. (2) one can also use a twin wire approximation, as described in [7].

* Work supported by GSI
# u.niedermayer@gsi.de

ISBN 978-3-95450-116-8

MAXWELL'S EQUATIONS AND FIT IN FD

A complete description of electromagnetic fields in FD is given by Maxwell's equations

$$\nabla \times \underline{\vec{E}} = \underline{\vec{J}}_m - i\omega \underline{\vec{B}} \tag{7}$$

$$\nabla \times \underline{\vec{H}} = \underline{\vec{J}}_e + \underline{\vec{J}} + i\omega \underline{\vec{D}} \tag{8}$$

$$\nabla \cdot \underline{\vec{D}} = \underline{\varrho}_e \tag{9}$$

$$\nabla \cdot \underline{\vec{B}} = \underline{\varrho}_m \tag{10}$$

and material equations

$$\underline{\vec{D}} = \underline{\varepsilon}(\omega)\underline{\vec{E}}, \quad \underline{\varepsilon} = \varepsilon' - i\varepsilon'' \tag{11}$$

$$\underline{\vec{B}} = \underline{\mu}(\omega)\underline{\vec{H}}, \quad \underline{\mu} = \mu' - i\mu'' \tag{12}$$

$$\underline{\vec{J}} = \kappa \underline{\vec{E}} \tag{13}$$

where $\underline{\varrho}_e$ and $\underline{\vec{J}}_e$ denote the electric source charge and current densities and $\underline{\varrho}_m$ and $\underline{\vec{J}}_m$ denote equivalent magnetic source charge and current densities, respectively. Magnetic currents will be used to imprint externally calculated boundary fields. The FIT discretization of Eqs. (7)-(13) in the discrete $\mathbb{C}^{3n_p}$ space (see e.g. [8]) are the so-called Maxwell-grid-equations (MGE)

$$\mathbf{C}\underline{\widehat{\mathbf{e}}} = \underline{\widehat{\mathbf{j}}}_m - i\omega \underline{\widehat{\mathbf{b}}} \tag{14}$$

$$\widetilde{\mathbf{C}}\underline{\widehat{\mathbf{h}}} = \underline{\widehat{\mathbf{j}}}_e + \underline{\widehat{\mathbf{j}}} + i\omega \underline{\widehat{\mathbf{d}}} \tag{15}$$

$$\widetilde{\mathbf{S}}\underline{\widehat{\mathbf{d}}} = \underline{\mathbf{q}}_e \tag{16}$$

$$\mathbf{S}\underline{\widehat{\mathbf{b}}} = \underline{\mathbf{q}}_m \tag{17}$$

with the diagonal material matrices containing the first to second order numerical approximations (second order only for homogeneous grid)

$$\underline{\widehat{\mathbf{d}}} = \mathbf{M}_\varepsilon \underline{\widehat{\mathbf{e}}} \tag{18}$$

$$\underline{\widehat{\mathbf{b}}} = \mathbf{M}_\mu \underline{\widehat{\mathbf{h}}} \tag{19}$$

$$\underline{\widehat{\mathbf{j}}} = \mathbf{M}_\kappa \underline{\widehat{\mathbf{e}}}. \tag{20}$$

The grid incidence matrix $\mathbf{C}$ is real valued and consists of the partial derivative incidence operators $\mathbf{P}_x, \mathbf{P}_y, \mathbf{P}_z$. Note that in contrast to Eqs. (7)-(10), the FIT equations do not require differentiability of the the continuous fields since they are based on an integral formulation. Without the magnetic charge and current, the curl-curl linear system is obtained

$$\left(\widetilde{\mathbf{C}}\mathbf{M}_{\mu^{-1}}\mathbf{C} + i\omega\mathbf{M}_\kappa - \omega^2\mathbf{M}_\varepsilon\right)\underline{\widehat{\mathbf{e}}} = -i\omega\underline{\widehat{\mathbf{j}}}_e. \tag{21}$$

In the following, the system will be symmetrically rewritten with $\underline{\widehat{\mathbf{e}}} = \mathbf{M}_\varepsilon^{-1/2}\underline{\widehat{\mathbf{e}}}'$as

$$(\mathbf{M}_\varepsilon^{-1/2}\widetilde{\mathbf{C}}\mathbf{M}_{\mu^{-1}}\mathbf{C}\mathbf{M}_\varepsilon^{-1/2} - i\omega\mathbf{M}_\varepsilon^{-1/2}\mathbf{M}_\kappa - \omega^2 I)\underline{\widehat{\mathbf{e}}}' = -i\omega\mathbf{M}_\varepsilon^{-1/2}\underline{\widehat{\mathbf{j}}}_e. \tag{22}$$

Equation (22) will be abbreviated by

$$\mathbf{A}\underline{\widehat{\mathbf{e}}}' = b. \tag{23}$$

EXCITATION TERMS

The monopolar excitation current is given as a discretization of (4) with constant σ as

$$\underline{\widehat{\mathbf{j}}}_{e,z}^{\mathrm{mono}}(i_z) = \int \underline{\vec{J}} \cdot \mathrm{d}\tilde{\mathrm{A}}_\mathrm{z} = \mathrm{q}\mathrm{e}^{-\mathrm{i}\omega \mathrm{z_i}/\mathrm{v}} \tag{24}$$

where i_z is the z-index and z_i is its z coordinate. The dipolar excitation current is modeled by the twin wire dipole approximation as

$$\underline{\widehat{\mathbf{j}}}_{e,z}^{\mathrm{dip}}(i_z) = \underline{\widehat{\mathbf{j}}}_{e,z}^{\mathrm{mono}}(x = -d_x) - \underline{\widehat{\mathbf{j}}}_{e,z}^{\mathrm{mono}}(x = +d_x). \tag{25}$$

The beam's charge in the dual volumina is obtained using the continuity equation

$$\begin{aligned}\underline{\mathbf{q}}_e &= \frac{i}{\omega}\widetilde{\mathbf{S}}\underline{\widehat{\mathbf{j}}} \\ &= \frac{i}{\omega}(e^{-i\omega\frac{\Delta z}{2v}} - e^{-i\omega\frac{-\Delta z}{2v}})\sigma e^{-i\omega z_i/v} \\ &= \frac{2\sigma}{\omega}\sin\left(\frac{\omega\Delta z}{2v}\right)e^{-i\omega z_i/v} = \frac{q\Delta z}{v}e^{-i\omega z_i/v} + O(\Delta z^3)\end{aligned} \tag{26}$$

for a longitudinally equidistant grid. The integral in the impedance definitions in Eqs. (5) and (6) is evaluated by the functional

$$Z(\underline{\widehat{\mathbf{e}}}(\omega)) = \underline{\widehat{\mathbf{e}}} \cdot \underline{\widehat{\mathbf{j}}}^* \tag{27}$$

with normalized magnitude of the current ($q = 1$ As).

2D SIMULATIONS AND BOUNDARY CONDITIONS

In general the electromagnetic field excited by moving charges can be split into a source and a scattered part (see e.g. [9]). Below the cut-off frequency of the connected PEC beam pipe one finds only the source field (including the space charge field) in the pipe since the scattered field decreases exponentially. For longitudinally homogeneous structures like the pipe stubs the Fourier correspondence $\partial_z \to -i\omega/v$ holds [1]. Therefore, two possibilities for the beam entrance and exit boundary conditions (BC) occur: A periodic BC in which the beam entrance and exit plane are mapped to each other or an infinite beam pipe BC in which the source field is calculated separately and imprinted as boundary condition on the right hand side of (23).

Phase Corrected Periodic BC

The phase of the field within the kicker vessel cannot be known a priori since it depends on the scattered field. Nonetheless, the total phase difference between the field on the entrance and exit of the beam is a priori given by the phase advance of the source field. Therefore one can transform the field from the entrance to the exit with the operator

$$P_{z,\mathrm{exp}} = e^{-i\frac{\omega(L+\Delta z_{\mathrm{exit}})}{\beta c}}, \tag{28}$$

ISBN 978-3-95450-116-8

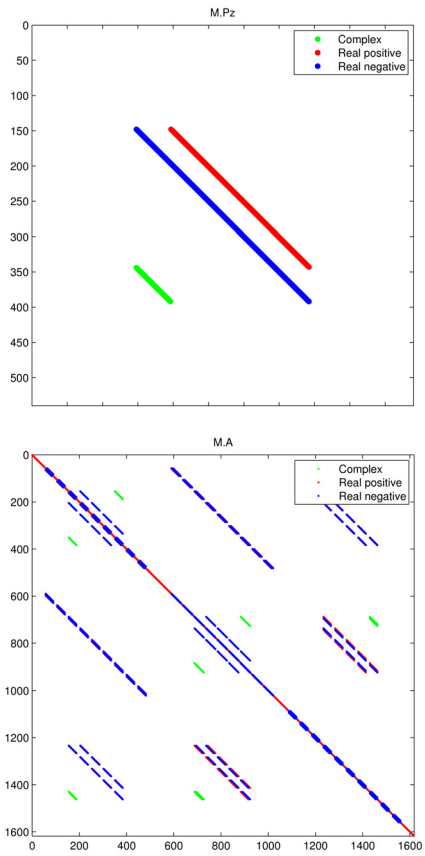

Figure 1: Sparsity pattern of $\mathbf{P}_z$ (top) and A matrix with periodic BC in z-direction and PEC-BC in x,y-direction (bottom). The green lines denote the factor $P_{z,\mathrm{exp}}$ which serves to close the curls on the z-boundary faces.

with L being the total length and Δz_{exit} being the length of the ghost edges at the exit. Drawbacks of these boundary conditions are that an additional band is introduced in the $\mathbf{P}_z$-matrix (see Fig. 1 top), leading to many additional bands in the curl-curl matrix (Fig. 1 bottom) and, more important, the main (large) curl-curl matrix is now complex.

Infinite Beam Pipe BC

For infinite beam pipe boundary conditions a supplementary grid (x,y-plane) has to be created on which the longitudinally harmonic fields are calculated and later imprinted in the right hand side of Eq. (23). We will refer to this as 2.5D solution since the longitudinal dependence is known a priori, but nonzero.

In the discrete formulation the grid incidence matrix for the longitudinal derivative is replaced by $\mathbf{P_z} = -\mathbf{1} + \exp(-\mathbf{i}\omega\triangle\mathbf{z}/\mathbf{v}) \approx -\mathbf{i}\omega\triangle\mathbf{z}/\mathbf{v}$. Note that $\widetilde{\mathbf{P}}_z = -\mathbf{P_z^H} = \mathbf{1} - \exp(+\mathbf{i}\omega\triangle\mathbf{z}/\mathbf{v}) \approx -\mathbf{i}\omega\triangle\mathbf{z}/\mathbf{v}$ is identical to $\mathbf{P_z}$ for small Δz. For the supplementary grid (SG) curl matrix one has $\widetilde{\mathbf{C}} = \mathbf{C}^H$. In the limit $v \to \infty$ which corresponds to $\partial_z \to 0$ the purely two-dimensional 'radial model' [1, 10] is found. Note that this simplified two-dimensional calculation serves not only as a boundary condition but also to calculate impedances of longitudinally homogeneous structures, as analytically done in e.g. [1, 7, 11].

The calculated 2D source fields are included in the main simulation by using the Source-Equivalence-Theorem. In practice this means that incomplete curls on the PEC-boundary are completed using the source field. One obtains (see also [9])

$$\begin{aligned}\mathbf{A}\underline{\widehat{\mathbf{e}}}' = &- i\omega\mathbf{M}_\varepsilon^{-1/2}\underline{\widehat{\mathbf{j}}}_e \\ &+ i\omega\mathbf{M}_\varepsilon^{-1/2}\underline{\widehat{\mathbf{j}}}_e^{\mathrm{eq}} - \mathbf{M}_\varepsilon^{-1/2}\widetilde{\mathbf{C}}\mathbf{M}_{\mu^{-1}}\underline{\widehat{\mathbf{j}}}_m^{\mathrm{eq}}. \end{aligned} \quad (29)$$

with the equivalent source electric and magnetic current densities given by

$$\underline{\widehat{\mathbf{j}}}_e^{\mathrm{eq}} = \widetilde{\mathbf{C}}_{\mathrm{R}}\underline{\widehat{\mathbf{h}}}^{\mathrm{SG}} \quad (30)$$

$$\underline{\widehat{\mathbf{j}}}_m^{\mathrm{eq}} = \mathbf{C}_{\mathrm{R}}\underline{\widehat{\mathbf{e}}}^{\mathrm{SG}} \quad (31)$$

where $\mathbf{C}_R$ and $\widetilde{\mathbf{C}}_R$ are the residual curl operators (the incidences missing in the main curl operator).

Space Charge Impedance as a Test-case

A verification of the implementation of the boundary conditions is given by the correct reproduction of analytically known space-charge fields and impedances for infinitely long beam pipes. In particular, the correct dependency on the velocity $\beta = v/c$ and mass factor $\gamma = (1-\beta^2)^{-1/2}$ of the beam show that the electric and magnetic fields cancel in the ultrarelativistic case. A mimetic correspondence from the FIT solution to the analytic calculation for a most simplified case can be found in the Appendix. Below the cut-off frequency, the correct $\beta^{-2}\gamma^{-2}$ dependence is found for both periodic and infinite beam pipe BC.

SOFTWARE

The CAD constructions and the mesh originate from CST EMS2011 [2]. It is imported via Matlab [12] where the material operators are disassembled in order to obtain the staircase material vectors. This allows to rescale the material parameters frequency dependently within the main program. Mesh data, material vectors and topological (PEC) information are transferred to the C++ main program. The actual high performance computations are carried out by the PETSc 3.2 [5] package which provides a variety of matrix structures, preconditioners and solvers for either real or complex linear systems. After computation, the fields can be visualized by transferring results back to Matlab and CST EMS2011. See Fig. 2 for the details. Equation (23) is treated with different PETSc solvers and preconditioners. So far, best results have been obtained by a symmetric successive over-relaxation (SSOR) preconditioner together with a stabilized bi-conjugate gradient (BICGSTAB), generalized minimum residual (GMRES) or a conjugate residual (CR) solver. In future, the application of algebraic multigrid (AMG) methods will be

ISBN 978-3-95450-116-8

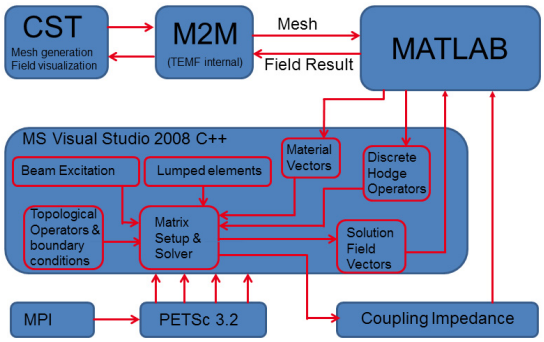

Figure 2: Implementation.

evaluated. For the supplementary grid, a direct solver (LU-decomposition) is applied since this does not constitute a bottleneck. For the main grid $3n_p = 10^6$ has been reached but the performance of the solver depends strongly on the frequency (diagonal dominance is a sufficient convergence condition for SOR). Note that the complex valued $\underline{\mu}$ deteriorates the condition number of the $\mathbf{A}$ matrix. For frequencies below the vessel cut-off (only $\approx$ 12 MHz due to the ferrite), the implementation of Doliwa's Neumann series approach [4] is considered.

APPLICATIONS

There is a variety of applications for this FD beam coupling impedance solver, especially the ones with ferrite are currently of interest. Ferrite materials provide high permeability (μ') but also high magnetization and polarization losses (μ'' and ϵ'').

Space Charge Compensation

The longitudinal space charge impedance (Eq. (40)) constitutes a major fraction of the imaginary part of the longitudinal impedance in SIS100. This leads to a RF-potential-well distortion and to a net decrease of the RF-voltage (decrease of bucket height). Since Eq. (40) behaves like a negative inductance, one has come up with the idea to compensate this with a lumped positive inductance, i.e. a cylindrical ferrite insertion. The ferrite has also the drawback of adding a major contribution to the real part of the longitudinal impedance. In the Los Alamos PSR one has found the 'Microwave Instability' occurring due to increased μ'' from the material [13]. Another issue is real-value of the transverse impedance added by the insert. With the presented simulation tool, the design and optimization of such an inductive insert can be approached. Figure 3 show the numerical calculation of a strongly simplified version of the insert. A way to avoid the instability could be to shield the insert from the beam at particular frequencies. Such shielding metal fingers are already in use in the LHC MKE-kickers [14].

Kicker with PFN

A major transverse impedance contribution in the SIS100 ring are the numerous ferrite kickers [15]. Besides

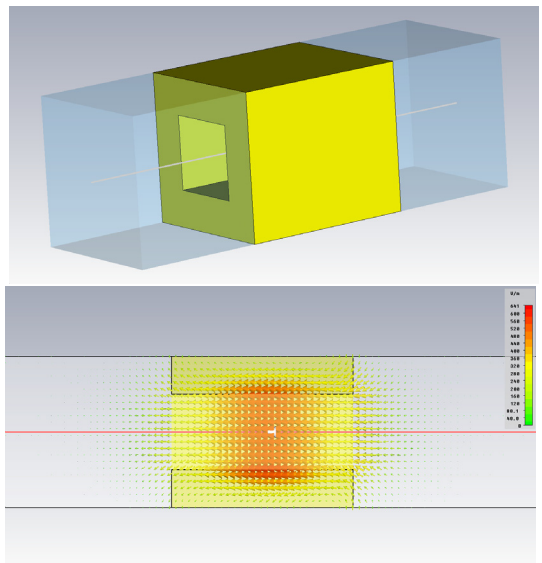

Figure 3: Simplified model of the insert with $\mu'_r = 1000, \mu''_r = 0$ (top) and electric field at $f = 100$ MHz with periodic boundary (bottom). The impedance is purely inductive.

the ferrite itself, also the supply network (pulse forming network, PFN) contributes to the impedance at lower frequencies. In the simulation the PFN can be included as a lumped admittance by adding its value to the correspondent entry in the $\mathbf{M}_\kappa$-matrix. The two frequency regimes in which the ferrite and the PFN dominate the transverse impedance are explained in [16]. There are means to shield the ferrite contribution [14] but the PFN impedance peaks are located partly within the kicker pulse spectrum, which cannot be shielded without interfering with the kicker's function (reciprocity).

CURRENT STATUS AND OUTLOOK

The fundamental part of the implementation of the code is done, the frequency range between 10 kHz and 100 MHz can be simulated with up to a few hundred thousand cells and either periodic or infinite beam pipe boundary conditions. In the near future, a divergence correction [17] using Eq. 26 will be implemented. At lower frequencies Doliwa's Neumann series approach [4] or an entirely two-dimensional simulation [1] are options. The presented software project aims for a complete database for the SIS100 longitudinal and transverse impedance below the beam pipe cut-off frequency. For the confirmation of the obtained results, bench measurements are outlined.

ACKNOWLEDGMENT

The authors wish to thank Wolfgang Ackermann for proofreading the manuscript.

ISBN 978-3-95450-116-8

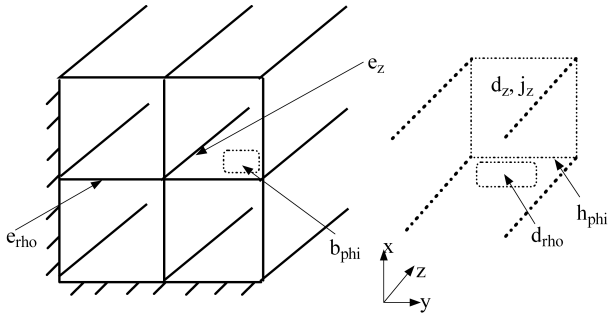

Figure 4: Simplest model mesh.

APPENDIX: SIMPLEST CASE FOR 2D CALCULATION

Applying the MGE (14)-(17) to the simplest structure in Fig. 4 one finds the following equations:

$$-i\frac{\omega}{v}\Delta z\underline{\widehat{\mathbf{e}}}_\varrho - \underline{\widehat{\mathbf{e}}}_z = -i\omega\underline{\widehat{\widehat{\mathbf{b}}}}_\varphi \tag{32}$$

$$4\underline{\widehat{\mathbf{h}}}_\varphi - i\omega\underline{\widehat{\widehat{\mathbf{d}}}}_z = \underline{\widehat{\widehat{\mathbf{j}}}}_{e,z} = q \tag{33}$$

$$-i\frac{\omega}{v}\Delta\tilde{z}\underline{\widehat{\widehat{\mathbf{d}}}}_z + 4\underline{\widehat{\widehat{\mathbf{d}}}}_\varrho = \mathbf{q}_e = \frac{q\Delta\tilde{z}}{v} \tag{34}$$

$$\underline{\widehat{\widehat{\mathbf{b}}}}_z = 0. \tag{35}$$

These three equations for the three unknowns $\underline{\widehat{\mathbf{e}}}_z$, $\underline{\widehat{\mathbf{e}}}_\varrho$ and $\underline{\widehat{\widehat{\mathbf{b}}}}_\varphi$ can be solved using the material operators (18) and (19),

$$\begin{aligned} 4\underline{\widehat{\mathbf{e}}}_z + \omega^2\mathbf{M}_\mu^\varphi\mathbf{M}_\varepsilon^z(\mathbf{I} - \frac{\Delta z\Delta\tilde{z}}{v^2}\mathbf{M}_{\mu^{-1}}^\varphi\mathbf{M}_{\varepsilon^{-1}}^\varrho)\underline{\widehat{\mathbf{e}}}_z \\ = i\omega\mathbf{M}_\mu^\varphi(\mathbf{I} - \frac{\Delta z\Delta\tilde{z}}{v^2}\mathbf{M}_{\mu^{-1}}^\varphi\mathbf{M}_{\varepsilon^{-1}}^\varrho)q \end{aligned} \tag{36}$$

where one obtains

$$(\mathbf{I} - \frac{\Delta z\Delta\tilde{z}}{v^2}\mathbf{M}_{\mu^{-1}}^\varphi\mathbf{M}_{\varepsilon^{-1}}^\varrho) = -\frac{1}{\beta^2\gamma^2}\mathbf{I} \tag{37}$$

independent of the mesh lengths. One finally finds

$$\underline{\widehat{\mathbf{e}}}_z = \frac{-i\omega}{4\beta^2\gamma^2 - \omega^2\delta_\perp^2/c^2}\mathbf{M}_\mu^\varphi q. \tag{38}$$

where $\delta_\perp = \Delta x = \Delta\tilde{x} = \Delta y = \Delta\tilde{y}$ denotes the transverse edges. Equation (36) is the mimetic correspondence to the continuous relativistic 2.5D Helmholtz equation [1]

$$\left(\triangle_\perp - \frac{\omega^2}{\beta^2\gamma^2c^2}\right)\underline{E}_z = -\frac{i\omega\mu\sigma}{\beta^2\gamma^2}e^{-i\omega z/v} \tag{39}$$

where the factor 4 in Eq. (36) originates from the difference stencil of the transverse Laplacian. From Eq. (39) one obtains after solving by a product separation ansatz and some simplifications [11] the longitudinal space charge impedance

$$\underline{Z}_\parallel^{SC} = -i\omega\frac{\mu_0 gl}{4\pi\beta^2\gamma^2}. \tag{40}$$

below cut-off. This behaviour ($\propto \beta^{-2}\gamma^{-2}$, $\propto \omega$, negative imaginary) has to be reproduced by the numerical solution, in particular by Eq. (38). Additionally, $\underline{Z}_\parallel^{\mathrm{SC}} \to 0$ must hold for $\omega \to \infty$. Note that the geometry factor g can only be poorly reproduced by staircase FIT for curved structures.

REFERENCES

[1] U. Niedermayer and O. Boine-Frankenheim, Analytical and numerical calculations of resistive wall impedances for thin beam pipe structures at low frequencies, NIM A 687, 5161, 2012.

[2] CST Studio Suite®2011/2012, www.cst.com

[3] K. Küpfmüller, Einführung in die theoretische Elektrotechnik, Springer, 1932.

[4] B. Doliwa et al., Optimised electromagnetic 3D field solver for frequencies below the first resonance, IET Sci. Meas. Technol., 2007

[5] Portable, Extensible Toolkit for Scientific Computation, www.mcs.anl.gov/petsc

[6] R. Gluckstern, Analytic methods for calculating coupling impedances, Cern Accelerator School, 2000.

[7] G. Nassibian and F. Sacherer, Methods for measuring transverse coupling impedances in circular accelerators, NIM, 1979.

[8] M. Clemens and T. Weiland, Discrete Electromagnetism with the Finite Integration Technique, PIER 32, 65-87, 2001.

[9] M. C. Balk, Feldsimulation starrer Teilchenstrahlen beliebiger Geschindigkeit und deren Anwendung in der Schwerionenbeschleunigerphysik, PhD at TU Darmstadt, 2005.

[10] H. Hahn, Matrix solution for the wall impedance of infinitely long multilayer circular beam tubes, PRSTAB 13, 012002, 2010.

[11] A. Al-Khateeb et al., Analytical calculation of the longitudinal space charge and resistive wall impedances in a smooth cylindrical pipe, Phys. Rev. E 63, 026503, 2001.

[12] MATLAB®R2011a, www.mathworks.de

[13] C. Beltran, Study of the longitudinal Space Charge Compensation and longitudinal Instability of the Ferrite Inductive Inserts in the Los Alamos Proton Storage Ring, PhD at Indiana University, 2003.

[14] T. Kroyer et al., Longitudinal and Transverse Wire Measurements for the Evaluation of Impedance Reduction Measures on the MKE Extraction Kickers, CERN AB-Note-2007-028.

[15] P. Spiller et al., FAIR Technical Design Report SIS100, 2008.

[16] B. Doliwa et al., Numerical calculation of transverse coupling impedances: Comparison to Spallation Neutron Source extraction kicker measurements, PRSTAB, 2007

[17] B. Doliwa and T. Weiland, Numerical Computation of Kicker Impedances: Towards a complete Database for the GSI SIS100/300 Kickers, Proc. of ICAP, 2006.

ISBN 978-3-95450-116-8